



Characterization of mechanical and bonding properties of anchoring resins under elevated temperature

Hadi Nourizadeh^{a,b,*}, Ali Mirzaghobanali^{a,b}, Kevin McDougall^c, L.H.J. Jeewantha^a, Peter Craig^d, Amin Motallebian^a, Behshad Jodeiri Shokri^{a,b}, Ashakan Rastegarmanesh^a, Naj Aziz^e

^a Centre for Future Materials (CFM), University of Southern Queensland, 4350, Australia

^b School of Engineering, University of Southern Queensland, 4300, Australia

^c School of Surveying and Built Environment, University of Southern Queensland, 4350, Australia

^d Jenmar Australia Pty Ltd, Sydney, Australia

^e School of Civil, Mining & Environmental Engineering, University of Wollongong, NSW, 2500, Australia

ARTICLE INFO

Keywords:

Rock bolts
Anchoring resin
Pullout tests
Bonding performance
Elevated temperature

ABSTRACT

Resin anchored rock bolts are widely used in the construction and mining industries to support and reinforce underground roadways and openings. However, increasing the depth of underground openings, particularly in coal mines, has presented a challenge for ground control designers due to the rise in geothermal heat and coal seam combustion. This study aims to comprehensively investigate the mechanical properties, microstructure, thermal and curing characteristics of the anchoring resins using Thermogravimetric Analysis, Dynamic Mechanical Analysis, and Differential Scanning Calorimetry tests. Pullout tests were conducted on resin encapsulated rock bolts to quantify their bonding performance at elevated temperatures ranging from 20 °C to 250 °C. The results showed that the mechanical properties of the resins are closely related to the type of curing agent, filler type and size, and curing time. The compressive strength and elastic modulus of the anchoring materials ranged from 51 to 103 MPa. DSC testing indicated that 65–83% of curing can be achieved in 30 min. At ambient conditions, good agreement was found between the compressive and shear properties of the anchoring resins and their corresponding bond resistance force. A heating and pull-out setup was fabricated to analyze the effects of temperature on the bonding performance of rock bolts chemically anchored in underground spaces. The results revealed a reduction in bonding capacity of the bolts by 6.6%–31.3% when the temperature of the environment reached 75 °C and 150 °C, respectively. The anchored bolts maintained up to 62.6% of their bonding resistance when the temperature increased to 250 °C. Temperature profiles measured by the thermocouples along the encapsulation length showed that the heat transition is independent of the resin type and more dependent on the rock bolt specification.

1. Introduction

Anchoring systems are commonly used for reinforcing and supporting ground and underground structures¹. These systems can be classified into three main categories: stranded steel tendons (cable bolts), deformed or threaded steel bars (rock bolts), and glass fiber reinforced polymer bars (GFRP). Rock bolting can be anchored either mechanically using an expansion wedge or shell or chemically using bonding agents. Chemically anchored rock bolts are typically inserted into a pre-drilled hole in the host media and filled with a structural bonding agent. The

function of the bonding agent is to transfer the anchoring load from the bolt to the surrounding rock mass and vice versa. There are two basic types of bonding materials: chemical and non-chemical. Cement-based materials, often called grout, are an example of non-chemical bonding agents and are not covered in this study. Unsaturated polyester resin (UPR), vinyl ester resin (VER), and epoxy resin are the most commonly used chemical bonding materials². UPR-based bonding products are widely used in mine support and building strengthening projects due to their shorter cure time, good bonding strength, and low cost³. The thixotropic and viscosity nature of polyester-based resins enhances their

* Corresponding author. Centre for Future Materials (CFM), University of Southern Queensland, 4350, Australia.

E-mail address: hadi.nourizadeh@usq.edu.au (H. Nourizadeh).

<https://doi.org/10.1016/j.ijmms.2023.105506>

Received 25 November 2022; Received in revised form 4 May 2023; Accepted 2 July 2023

Available online 6 July 2023

1365-1609/© 2023 The Authors. Published by Elsevier Ltd. This is an open access article under the CC BY-NC-ND license (<http://creativecommons.org/licenses/by-nc-nd/4.0/>).

workability for various applications, although this group offers lower bonding capacity compared to vinyl ester and epoxy resins. The degradation process of UPR and VER under different conditions, such as exposure to chemicals, microwave radiation, and high temperature, has been studied, and it has been established that immersion in aggressive solvents and exposure to higher temperatures (e.g., 1000 °C) degrade and carbonize the matrix, while UV radiation causes additional cross-linking in the resins⁴. For anchor bonding applications, anchor resins can be distinguished by vial (two-component cartridge) and injection systems. The two-component cartridges typically consist of a tube of polyester film filled with polyester resins and a curing agent (catalyst), which is usually a peroxide like methyl ethyl ketone peroxide or benzoyl peroxide. A film barrier of polyester is used to prevent migration between the resin and the hardener. Inorganic fillers such as calcium carbonate (CaCO₃) and silica are usually added to the resin components to enhance the mechanical properties and minimize expenses. Several studies have been conducted to investigate the effect of filler content and particle sizes on the mechanical properties of polyester resins, and it has been reported that mechanical and bonding properties of resins can be enhanced by incorporating an optimum content of filler^{5–8}.

The behavior of resin-encapsulated anchors can be viewed from two perspectives: short-term properties, including gelling time, setting time (early curing time), and early bonding strength; and long-term properties, including bearing capacity against static and dynamic loads, and resistance to harsh and corrosive environments, temperature, and fire. The chemical formulation of resins is a critical characteristic, along with other parameters such as host rock mass condition, level of in-situ stress, and mechanical and geometric specifications of the anchoring element, which influence the performance of rock bolting systems. Curing of thermosetting resins is an exothermic and time-dependent chemical reaction that occurs once the components (resin and curing agent) are mixed. Gelation is an important factor achieved when the chemical reaction proceeds sufficiently such that the mixture achieves a flexible but non-flowing three-dimensional high molecular structure. The gel time, early and fully curing time, and viscosity of the product influence the suitability of chemically anchored rock bolts for particular applications⁹.

There is a broad range of literature on the experimental and numerical investigation of the effects of different factors, such as mechanical properties of anchoring materials, confining stress, anchoring materials mixing and installation procedure, and rock bolt geometrical and mechanical properties, on the bond behavior of fully encapsulated rock bolts in ambient conditions^{10–18}. Huang et al.¹⁹ concluded that Basalt FRP bars anchored with resin with a higher elastic modulus have higher shear stiffness compared to the bars anchored with a lower elastic modulus. Pull-out tests conducted by Dudek and Kadela²⁰ on chemically bonded steel bars showed that the bearing capacity of the bars bonded by epoxy adhesive is slightly higher than those bonded using polyester resins. The results of various studies also show that mechanical characteristics of grout play a vital role in determining the bearing capacity of rock bolts and cable bolts^{14,21–23}.

Previous research studies have shown that the mechanical properties and load-bearing capacity of anchoring resins depend on temperature. Wang et al.²⁴ examined the effects of high temperature and low humidity on the mechanical properties of grouting materials in high-geothermal tunnels. They found that these factors have an adverse effect on cementitious grout. Jahani et al.²⁵ experimentally studied the influence of temperature on the mechanical properties of a structural adhesive and found that the mechanical properties decrease when the curing and post-curing temperature exceeds the glass transition temperature (T_g) of the adhesive. T_g is defined as the temperature range at which the state of a thermosetting resin changes from a glassy state to a rubbery state²⁶. Previous research has shown that commonly used structural agents have T_g in the range of 40–70 °C, and their mechanical properties substantially change when the working temperature

approaches the corresponding T_g ^{27,28}. It has been shown that for temperatures below 60 °C, the properties of chemical bonding agents are slightly affected. However, for temperatures above 60 °C, there is a significant reduction in bonding properties. Reis²⁹ measured the elastic modulus, flexural strength, and compressive strength of polymer mortars under different temperatures and concluded that the flexural and compressive strength decrease at elevated temperatures.

To characterize the bonding behavior of an encapsulated bolt in thermal environments, two sets of data are essential: the temperature distribution along the encapsulation length and the relationship between induced bond stress and temperature. The temperature profile along the bonded length is a time-dependent factor, but the testing configuration and method also affect the temperature distribution profile. There is limited literature regarding the investigation of the effects of elevated temperature on the bonding properties of chemically bonded anchors in concrete structures, particularly in underground applications. The experimental procedures and standards developed for investigating the performance of reinforcing materials in concrete structures under elevated temperature may not be suitable for underground applications because the conditions vary significantly. Temperature rises in underground spaces, such as tunnels and mines, can be due to fire, combustion, machine working, and geothermal heat. In concrete structures, the temperature elevation in the bond is closely dependent on the geometry of the concrete structure³⁰. In underground structures, only the free end of the reinforcing element and the external fixtures are exposed to the ambient heat, regardless of the geometry of the opening (except in the presence of geothermal heat, which is transmitted from all directions). In determining the resistance to heat of rebars in concrete structures, the main thermal flux is usually subjected to the lateral sides of the concrete specimens^{31,32}. The European Organization for Technical Assessment (EOTA) outlines that “The main thermal flux shall be oriented towards the lateral side of the concrete cylinder. The non-bonded part of the rebar shall not be directly exposed to the heat source”³³. Al-Mansouri et al.³² and Lakhani and Hofmann³⁴ observed a large difference in the temperature variation along the encapsulation depth for the specimens where the bolt itself was exposed to heat compared to the specimens where the bolt was insulated.

The literature reports that the mechanical and thermal characteristics of UP, VE, and epoxy, with various formulations of matrix, filler, and other additives, have been well-studied under different environmental and testing conditions^{35–43}. However, the literature lacks comprehensive studies that evaluate the axial performance of resin-embedded rock bolts at higher temperatures, which could simulate the underground conditions where the bolts are installed. This paper presents a qualitative and quantitative discussion of the mechanical and thermal characteristics and behavior of commonly used anchoring UP resins. Additionally, the bearing performance of encapsulated rock bolts was investigated under elevated temperatures in simulated underground heating conditions. Furthermore, the interrelationship between the bearing capacity of rock bolts under ambient and elevated temperature conditions and the thermo-mechanical characteristics of the anchoring materials was examined, and the relevant failure patterns were analyzed. As previously stated, the conventional testing procedure developed for evaluating the effects of high temperatures on the performance of anchoring materials in concrete structures is not suitable for underground structures. To address this incompatibility, a new testing set-up was designed to mimic the conditions of these environments. The outcomes of this study may aid in developing standard testing methods for reinforcing materials used in underground applications. Moreover, the results of this study may inform the design and construction of more efficient and reliable rock support systems, leading to safer and more efficient underground excavations. Importantly, extending the depth of underground openings, particularly coal mines, increases the geothermal heat and combustion of coal seams, posing a challenge for ground control designers. Therefore, understanding the performance of anchoring materials at higher temperatures is crucial.

2. Experimental procedure

2.1. Materials

The study employed four types of two-component polyester resins (denoted as resins A, B, C and D), specifically synthesized for rock bolting, as the bonding agent. The polyester resin component of these resins contained styrene monomer and was filled with CaCO₃ inert fillers of various particle sizes, ranging from 0.5 μm to 1300 μm. Two types of curing agents, a water-based and an oil-based catalyst, were utilized in the research. Both catalysts contained the same limestone filler but differed in the amount of benzoyl peroxide initiator. The specific mixing ratios of the resins and the catalysts are presented in Table 1. The resins were catalyzed using 20% w/w and 8% w/w of water-based and oil-based catalysts, respectively, as shown in the table. The components of the bonding resins used in this study are illustrated in Fig. 1.

2.2. Experimental program

The testing program was divided into three stages. In the first stage, the mechanical properties of the bonding agents, including their compressive, tensile, and shear characteristics, were determined. The compression test was conducted on specimens cured for 1 h, 1 day, 3 days, and 30 days to investigate the effect of curing time, while tensile and shear tests were only performed on specimens cured for 30 days. In the second stage, microstructural analysis of the failure surfaces obtained from the mechanical experiments was carried out, along with thermal analysis, including thermogravimetric analysis (TGA), differential scanning calorimetry (DSC), and dynamic mechanical analysis (DMA). This investigation was conducted to study the decomposition, storage modulus, curing rate, and T_g, which are important factors to consider when assessing the effect of temperature on the behavior of materials. The TGA and DMA tests were performed on specimens cured for 30 days, while the DSC test was carried out on uncured specimens and specimens cured for 0.5 h, 1 h, 24 h, 7 days, and 30 days. The DSC analysis was undertaken at different curing times to accurately quantify the curing percentage of the resins after mixing with the catalysts. The third stage of this experimental study investigated the bonding behavior and anchoring capacity of rock bolts under both room and elevated temperatures. As this study targeted the underground application of reinforcing materials, testing setups used in the literature were not considered suitable. Therefore, a unique heating and testing setup was developed to simulate the desired elevated temperature conditions. Pull-out tests were then conducted on the bonded rock bolts at room conditions and elevated temperatures of 75 °C, 150 °C, and 250 °C.

2.3. Mechanical tests

All the specimens for the mechanical, thermal, and pull-out analyses were prepared by mixing the main components of the resins using a

Table 1
Resin components used in the study.

Items	Type A	Type B	Type C	Type D
Matrix resin	Polyester Resin	Polyester Resin	Polyester Resin	Polyester Resin
Filler	CaCO ₃	CaCO ₃	CaCO ₃	CaCO ₃
Filler particle size (μm)	10–425	0.5–425	10–1300	10–1300
Bulk density of resin mastic (kg/m³)	1817	1746	1790	1795
Curing agent	Water-based	Oil-based	Water-based	Oil-based
Mixing mass ratio (resin: catalyst)	4:1	11.5:1	4:1	11.5:1

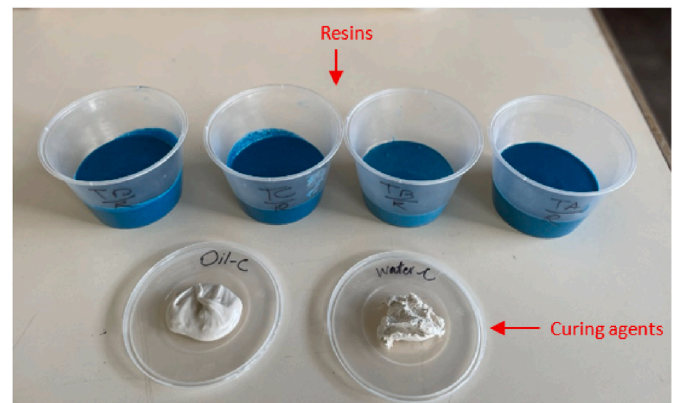


Fig. 1. Bonding resins components used in this study.

laboratory mixer. The mixing process was carried out in a room with a temperature-controlled system set at 20 °C, and the mixing time and speed were set to 30 s and 500 rpm, respectively. Immediately after the mixing process was completed, the uncured resins were poured into the designated molds. The specimens were then demolded after 30 min and stored in a temperature-controlled environment at 20 °C to complete the curing process. The specimens were tested at the scheduled curing time frames. Table 2 summarizes the details of the mechanical tests performed on the specimens. The tests were executed following the ASTM standards listed in Table 2. To verify the accuracy and consistency of the results, the tests were repeated for each type of resin at the desired curing period (refer to Table 2). Conventional resistive strain gauges were used to instrument the specimens in compressive and tensile tests to measure the respective lateral and axial strains, and consequently calculate the compressive and tensile elastic modulus and Poisson's ratio. The tensile and V-notched shear (Iosipescu) tests were conducted using a 100 kN hydraulic servo-controlled MTS machine. A Wyoming shear testing fixture was used for the V-notched shear specimens. However, the compressive tests were performed using a 1000 kN hydraulic servo-controlled UTM machine due to the need for higher load before yielding. Fig. 2 illustrates the mechanical testing of the specimens.

2.4. Microstructural and thermal analysis

The morphology of the specimens was observed using a Jeol Benchtop (JCM-6000) Scanning Electron Microscope (SEM). Non-isothermal analyses were also performed to determine the curing percentages, using a TA Instrument Discovery DSC-25. The uncured and cured samples (taken at 0.5 h, 1 h, 1 day, 7 days, and 30 days) were heated from 0 °C to 150 °C with a constant heating rate of 5 °C/min. For the DSC experiments, ~12 ± 0.1 mg of the sample was loaded into hermetically sealed aluminum pans using a manual crimper. Thermogravimetric analysis was carried out using a TA Instruments Discovery SDT 650. The temperature was raised from room temperature to 600 °C at a rate of 5 °C/min. Dynamic Mechanical Analysis (DMA) was conducted in accordance with ASTM D7028 standard, using a TA Instrument Hybrid Rheometer (Discovery HR-2). Rectangular specimens, with dimensions of 60 mm (L) × 12 mm (W) × 4 mm (T), were clamped in a dual cantilever fixture. Before beginning the test, the specimens were conditioned at 0 °C for 15 min, and then heated with a 5 °C/min rate until 120 °C under an oscillation mode at a frequency of 1 Hz. Fig. 3 illustrates the equipment and specimens used for the thermal analysis.

2.5. Pull-out tests under elevated temperatures

For the pull-out experiments, steel rock bolts with a nominal diameter of 22 mm (rib-to-rib), fully bonded in steel pipes with an outer

Table 2
Mechanical tests parameters.

Test	Curing age	Standard	Dimensions L × W × T (mm)	Geometry	N _R ^c	N _T ^d	Loading rate
Compressive	1h, 1day, 3days, 30days	ASTM:C579	50 × 50 × 50	Cubic	3	48	1.5 kN/s
Tensile	30days	ASTM:D638	120 × 10 × 10 ^a	Dog bone	5	20	1 mm/min
Shear	30days	ASTM:D5379	76 × 20 × 10 ^b	V-notched	5	20	1 mm/min

^a Width at the middle of the specimens.

^b The widths of the specimen at the notch is 11 mm.

^c N_R: number of the tests at each testing group.

^d N_T: total number of the tests.

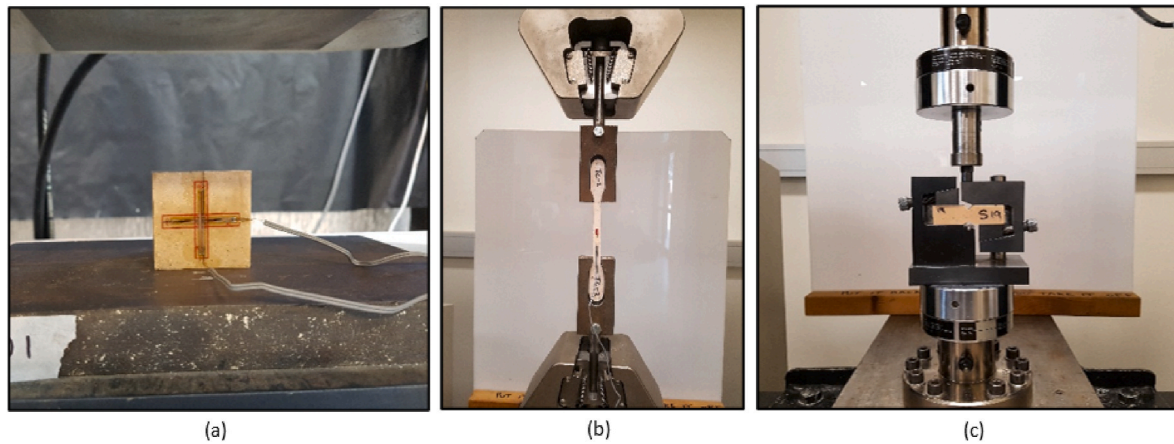


Fig. 2. Mechanical testing, (a) compressive (b) tensile and (c) V-notched (Iosipescu).

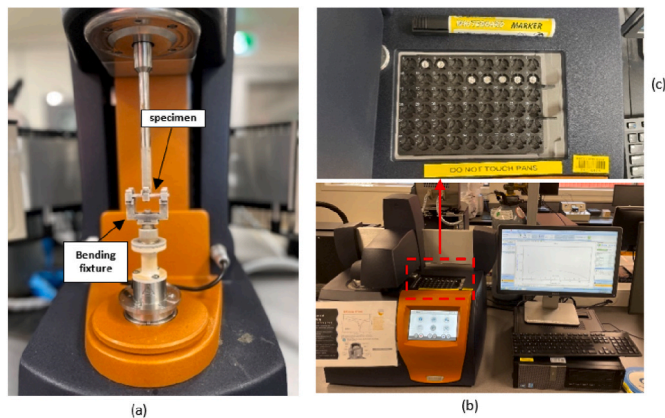


Fig. 3. Thermal analysis instruments, (a) Discovery HR-2, (b) DSC-25 and (c) DSC specimens in designated tray.

diameter of 43 mm, thickness of 5 mm, and length of 150 mm, were used. The rock bolts had a yield strength of 650 MPa, a tensile strength of 890 MPa, and an elastic modulus of 220 GPa. The pipes were rifled internally to mimic field conditions and ensure debonding occurred either in the bonding materials or at the bolt-resin interface. Freshly mixed resins were poured into the pipes, and the rock bolts were centrally installed using designated and fabricated centralizing tools. The specimens were stored at room temperature. The first set of experiments was conducted at room temperature, while the second group of tests was performed at elevated temperatures. To simulate rock bolt performance in underground applications, specialized heating and testing equipment was designed and fabricated. This consisted of an insulated heating chamber with a temperature range of 50 °C–400 °C. Thermocouples measured the system temperature and provided feedback to the control system. Once the chamber was installed under the middle crosshead of the 1000 kN UTM, the specimen was placed under the chamber by

passing the bolt through the designated 40 mm hole in the center of the heating chamber. The free end of the rock bolts was clamped by the conical jaws located on the upper crosshead of the 1000 kN UTM. The middle crosshead was then adjusted so that the upper side of the steel pipe sat underneath the chamber. Three k-type thermocouples (named T1, T2, and T3) were positioned along and on the bolt at 30 mm, 80 mm, and 130 mm from the loading end. One thermocouple (T0) was attached to the bolt, 15 mm outside the encapsulation surface. The chamber was heated from room temperature to the set temperature at a rate of 10 °C/min. The specimen was kept at the set temperature for 30 min, and then the pull-out load was applied at a rate of 1 mm/min until debonding occurred. Table 3 and Fig. 4 illustrate the pull-out test experimental array and the pull-out experimental setup, respectively.

3. Results and discussion

3.1. Mechanical properties

In this section, the results obtained from the mechanical testing will be presented and discussed.

Table 3
Pull-out test experimentation.

Bonding type	Encapsulation length (mm)	Testing temperature (°C)	Number of tests	Exposure time to the desired temp (min)
Type A	150	24 ^a , 75, 150, 250	4	30
Type B	150	22 ^a	1	n/a
Type C	150	22 ^a	1	n/a
Type D	150	20 ^a , 75, 150, 250	4	30

^a Room temperature.

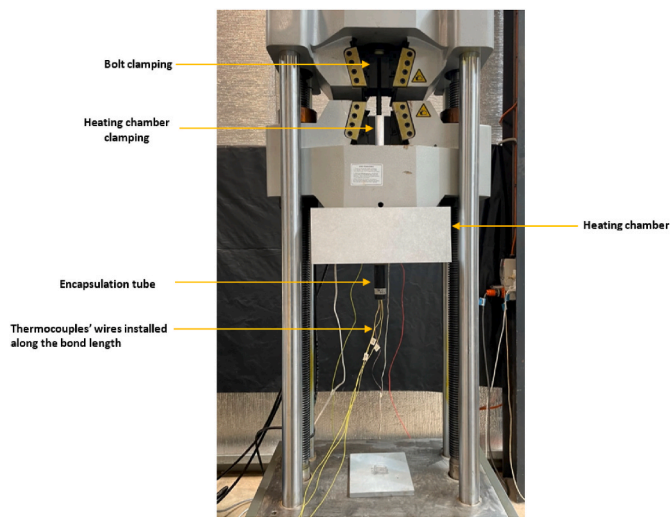


Fig. 4. Pull-out testing set-up.

3.1.1. Compressive properties

Table 4 presents a summary of the compressive test results after 30 days. Resins A and C showed the lowest compressive strength and elastic modulus. This is believed to be due to the challenge of effectively mixing water-based additives, which can create voids and defects in the cured specimens. The failure surface images of the specimens (Fig. 5) indicate that resins A and C have more porosity compared to resins B and D. Since the mechanical behavior of solids is often governed by flaws, it is reasonable to conclude that under compression, localized tensile stress is initiated at the defects, leading to crack propagation and eventual material failure. Microstructural effects, such as voids and second-phase particles (such as fillers and fibers), are the primary reasons for crack initiation and development in polymeric materials under compressive load⁴⁴.

Resin D exhibited an 86% higher compressive strength than resin C, despite using the same matrix resin and filler type and size, suggesting that the improvement is linked to the type of catalyst. Table 1 and Table 4 suggest that filler particle size also affects the mechanical properties of chemical bonding materials. Resin C demonstrated slightly higher compressive strength than resin A (~5.3%) despite using the same type and ratio of curing agent. The same trend was observed in resins B and D, where resin D exhibited higher compressive and elastic modulus than resin B (~9.9%), possibly due to a wider CaCO₃ particle size distribution in resin C. Bagherzadeh et al.⁷ noted that combining fillers with different particle sizes can enhance the compressive strength of anchoring bonds. When there is a sufficient amount of resin present, the voids are typically filled completely, resulting in maximum stress. Generally, finer particle sizes lead to higher strength properties of composite materials in particular tensile and flexural strengths³⁷. The compressive tests conducted in the current study indicate that samples with a wider particle size distribution resulted in slightly stronger resin compared to those with a narrow particle size. This could be due to

Table 4
Summary of the 30-day compressive tests.

Resin type	Resin A	Resin B	Resin C	Resin D
Ultimate Strength (MPa)	51.78 ± 0.51	93.78 ± 0.97	54.55 ± 1.65	103.05 ± 1.51
Young's Modulus (GPa)	4.71 ± 0.09	7.45 ± 0.06	4.78 ± 0.1	8.03 ± 0.07
Poisson ratio	0.22 ± 0.01	0.28 ± 0.02	0.23 ± 0.01	0.36 ± 0.04
Strain at ultimate strength (10 ⁻²)	1.112	1.274	1.491	1.561

several factors, such as (1) a wider particle size distribution allows for more efficient packing of filler particles in the resin matrix, leading to a denser material with fewer voids and gaps, (2) the use of larger particles may result in a greater degree of interlocking between the particles in contact, and (3) a wider range of particle sizes may result in a more uniform distribution of filler particles within the resin matrix. Yeon et al.⁴⁵ reported a slight increase in the compressive strength of UPR polymer concrete with increase in the size of spherical filler particles. The compressive strength and elastic modulus of resin A were found to be the lowest among the tested resins, measuring 52 MPa and 4.71 GPa, respectively. On the other hand, resin D exhibited the highest compressive strength and stiffness. Its ultimate compressive strength and elastic modulus were measured to be 103 MPa and 8 GPa, respectively. This resin contained a wider range of filler particles and an oil-based curing agent, which resulted in higher strength and stiffness compared to the other resins. Fig. 6 depicts the compressive stress-strain curves of the specimens tested at room temperature. The compressive behavior of the specimens, as shown in Fig. 6, resembles the deformation process of quasi-brittle materials, which involves an elastic phase, strain hardening, peak stress, strain softening, and a sharp decline in stress⁴⁶. All specimens exhibit linear stress-strain behavior in the elastic zone until approximately 85% of peak stress. At the end of this stage, peak stress is achieved, which is associated with specimen failure followed by a sudden decline in stress. At this stage, the absorbed energy is released suddenly in the form of crack propagation. This behavior is comparable to the post-peak behavior of brittle materials due to the sudden reduction in stress^{47,48}. The maximum compressive stress was obtained at true strains of 1.1%, 1.2%, 1.49%, and 1.56% for resins A, B, C, and D, respectively. The Poisson ratio of the resins was also determined using the strain values obtained from strain gauges. It can be observed from Table 4 that the Poisson ratio ranges from 0.22 to 0.36.

Fig. 7 depicts the compressive stress-deformation curves for curing times of 1 h, 1 day, 3 days, and 30 days. It is evident that the compressive behavior of the tested anchoring resins is influenced by their curing time. Chen et al.⁴⁹ have identified five distinct stages of typical compressive stress-strain behavior for polymers: linear elastic stage, nonlinear elastic stage, yield-like (peak) stage, strain softening stage, and perfectly plastic behavior stage. Resins A and C cured for 1 h exhibited all five stages, while resins C and D cured for 1 h displayed only the first two stages followed by a strain hardening stage, with significant deformation occurring with slight increases in stress. As shown in Fig. 7, resins B and D exhibited ductile behavior for specimens tested at 1 h, whereas resin A displayed quasi-ductile behavior and resin C behaved like a typical polymer (elastic-yield (peak)-softening-plastic behavior). The stress of resins B and D slightly decreased after reaching 2.6% strain, while the limit was 1.7% for resins A and C tested at 1 h (Fig. 7). No distinct ductile-brittle transition point was observed in the post-peak region for specimens tested at 1 h.

A comparison of the stress-deformation curves presented in Fig. 7 indicates that the degree of ductility is a function of time and the catalyst type used. It can be concluded that the compressive stress-strain relationship of resins changes from ductile behavior at the early stages of curing (e.g., resin B and D at 1 h) to a quasi-brittle behavior when it hardens (e.g., resins A, B, C, and D at 30 days). Furthermore, it is clear that the resins with oil-based catalyst components (i.e., resins B and D) exhibit more ductility compared to the ones with water-based catalysts (i.e., resins A and C). This indicates that the curing process is faster in resins A and C in which the water-based catalyst was used. The curing degree of the specimens over time is described in detail later in Section 3.2. Resin B tested at 1 day and D tested at 1 day and 3 days still illustrate strain hardening behavior after the yielding point. Elastic-yield like (peak)-strain softening behavior presented in resins A and C at 1 day, 3 days, and 30 days, resin B at 3 and 30 days, and resin D at 30 days, is similar to the stress-strain behavior of polymer concrete with a high proportion of fly ash⁵⁰. The basic response of the four specimens at the late stages of curing as shown in Fig. 7 is nearly identical. However, a

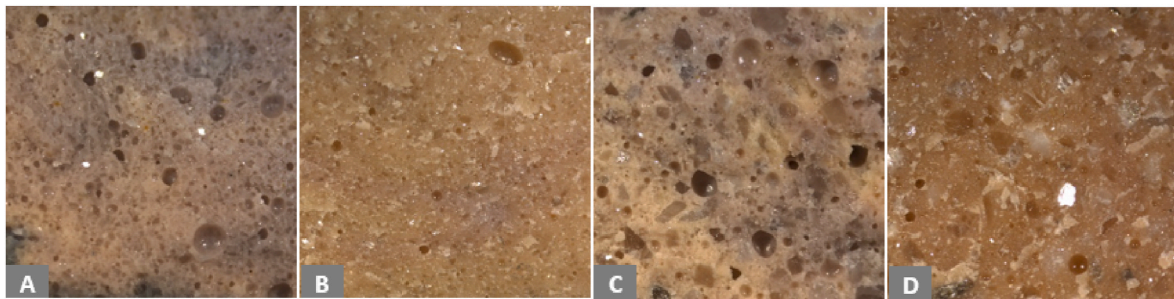


Fig. 5. Failure surface of the specimens from mechanical tests.

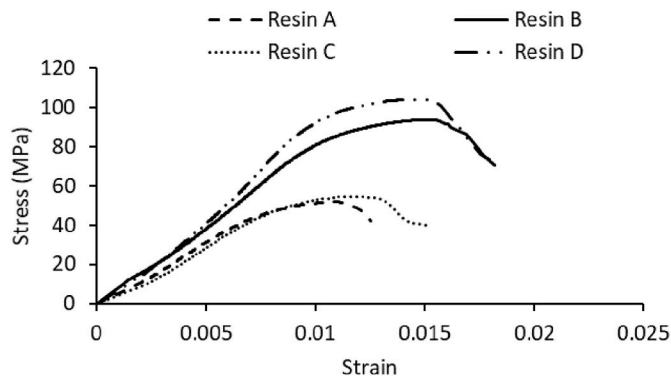


Fig. 6. Stress-strain behavior of different resin specimens tested at 30 days.

comparison of the stress-strain curves reveals that the descending rate of stress at the post-yield strain softening stage is greater at higher curing stages.

The results of the compressive tests conducted on different types of resins over time are summarized in Table 5 and Fig. 8. It is observed that the ultimate compressive strength and elastic modulus of the resins increase with curing time. For example, the compressive strength of resin A improved by 20%, 33%, and 57% after 1 day, 3 days, and 30 days of curing, respectively, compared to the 1-h specimen. Resin B exhibited an improvement of 43%, 56%, and 96%, while resin C and D showed an improvement of 35%, 53%, and 89%, and 40%, 66%, and 119%, respectively. This development in compressive strength is attributed to the curing of the resins, and the results indicate that the water-based catalyst promoted a faster hardening process at the very early stage of curing compared to the oil-based catalysts. In cases where strain hardening is not observed, the yield strength and peak strength become equivalent.

Fig. 9 depicts the macroscopic failure patterns of the specimens subjected to compression over different curing periods. In most cases, a cone-shaped rupture is clearly visible, but in a few cases (e.g., 1-h C, 1-Day B, and 1-Day D), debris covers the failure mode. The wedge in the compressive specimens forms an angle of approximately 45° with the vertical side of the specimen. In all specimens, failure began with a

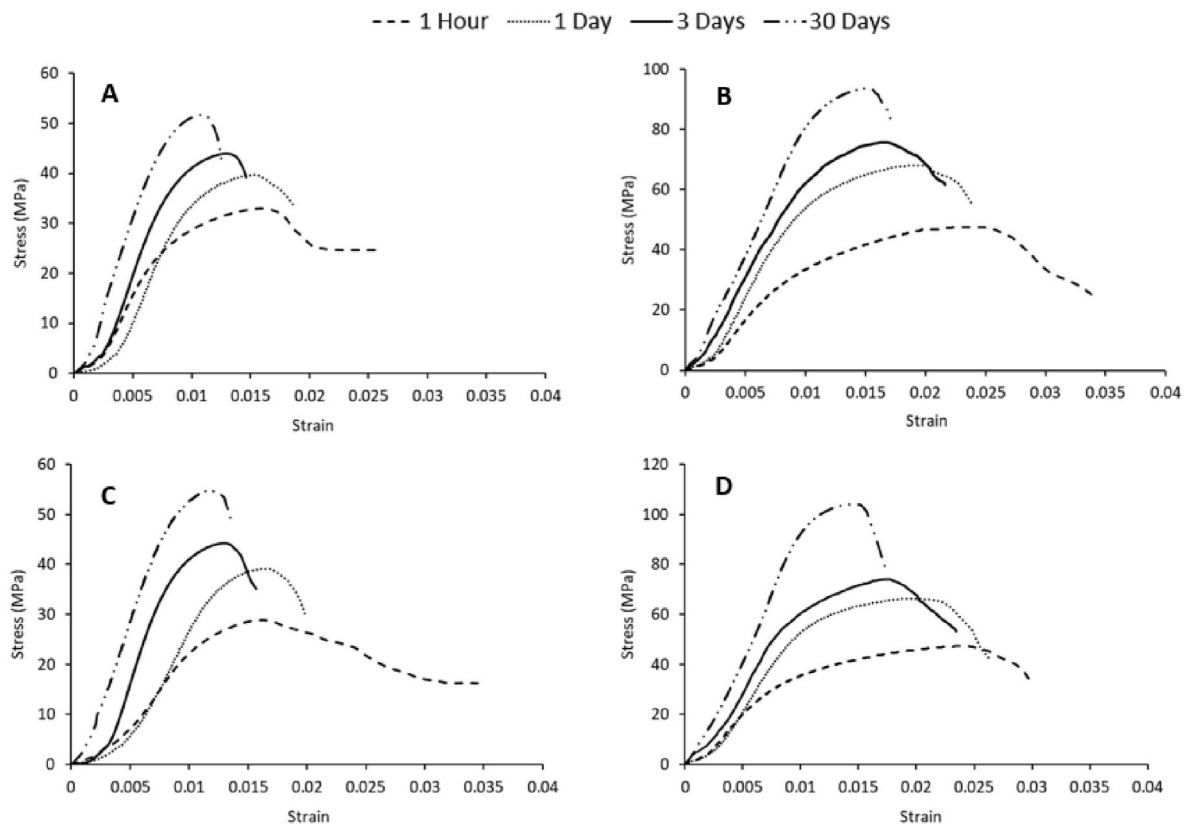


Fig. 7. Stress-deformation behavior of the resins at different curing ages.

Table 5
Compressive results over curing periods.

Resin Type	Parameters	1 Hour	1 Day	3 Days	30 Days
Resin A	Peak Strength (MPa)	32.9	39.6	43.9	51.7
	Yield Strength (MPa)	28.9	39.6	43.9	51.7
	Young's Modulus (GPa)	3.06	2.84	3.99	4.71
	Strain at yield (10^{-2})	1.02	1.52	1.33	1.12
	Strain at peak (10^{-2})	1.67	1.52	1.33	1.12
Resin B	Peak Strength (MPa)	47.6	68.1	74.6	93.7
	Yield Strength (MPa)	38.5	60.3	74.6	93.7
	Young's Modulus (GPa)	3.68	5.39	6.01	7.45
	Strain at yield (10^{-2})	1.28	1.22	1.61	1.5
	Strain at peak (10^{-2})	2.53	1.99	1.61	1.5
Resin C	Peak Strength (MPa)	28.8	39.1	44.3	54.6
	Yield Strength (MPa)	28.8	39.1	44.3	54.6
	Young's Modulus (GPa)	1.83	2.15	3.73	4.78
	Strain at yield (10^{-2})	1.63	1.67	1.33	1.18
	Strain at peak (10^{-2})	1.63	1.67	1.33	1.18
Resin D	Peak Strength (MPa)	47.3	66.3	78.6	103.9
	Yield Strength (MPa)	36.6	58.1	78.6	103.9
	Young's Modulus (GPa)	4.09	5.50	6.52	8.03
	Strain at yield (10^{-2})	1.06	1.18	1.68	1.48
	Strain at peak (10^{-2})	2.44	2.24	1.68	1.48

bulging deformation in the middle of the specimens, followed by the final cone-shaped failure. However, the degree of initial bulging varied based on the resin type and curing age. For example, among the specimens tested after 1 h, the resin D specimen exhibited the greatest degree of bulging, while the lowest degree was observed in resin A. The deformation measured in the middle of the specimens using mounted strain gauges indicated that the lateral deformation in specimen D before failure was greater than that of specimen C, which may result in a higher Poisson ratio for resin D tested at 1 h, as well as a higher degree of bulging compared to the other resins. Furthermore, the lateral strain values recorded during uniaxial loading exhibited a gradual reduction in the degree of bulging with increasing curing duration. After 1 day, the bulging was significantly reduced for resins A and C compared to resin B, and particularly for resin D. These failure patterns can be related to the post-yield stress-strain relationship presented in Fig. 7. Since the bulging deformation is greater in resins B and D than in resins A and C, it is assumed that post-yield hardening leads to greater bulging deformation. It should be emphasized that in all specimens, the bulging shape deformation was formed before the peak stress, after which cone-shaped failure occurred suddenly. Under compressive loading, the cross-sectional area of the specimen close to the loading platens tends to increase; however, frictional forces between the top and bottom surfaces of the specimens and the platens hinder the outward deformation, while the specimens at the middle expand outwardly when unconstrained. This deformation scheme leads to an initial bulging profile with the internal regions remaining unreformed, followed by a cone-shaped failure (Fig. 10).

3.1.2. Tensile properties

The results of the tensile tests are presented in Fig. 11. All types of resin exhibited a brittle behavior with nearly the same response. The stress-strain curves indicate that for resins A and C, stress increases linearly until reaching the ultimate tensile stress, whereas for resins B and D, the stress initially increases linearly and then is followed by a slight non-linear deformation. Table 6 summarizes the values of peak stress, corresponding strain, and elastic modulus. The results indicate that resin B exhibited the highest strength of 10.81 MPa, while resin D exhibited the highest elastic modulus ($E = 20.76$ GPa) in the tensile tests. The lowest values of tensile strength and modulus were recorded for resin C, which measured 7.29 MPa and 6.79 GPa, respectively. Comparing the results of the compressive tests (refer to Section 3.1.1) and the tensile tests shows that the strongest resin in compression does not necessarily offer the highest tensile strength. Similar to the compressive behavior, the tensile behavior of the resins is related to the particle size of the filler and the curing catalyst. The oil-based catalyst showed higher strength in tension due to the lower volume of imperfections, such as voids. In compression, particles ranging from micro to millimeter improved the strength; however, fine particles showed better tensile results. Similar effects of particle size on the tensile properties of thermosetting resins have been previously reported, where finer spherical filler particles of $CaCO_3$ presented higher strength due to a more efficient stress transfer mechanism. Mourad et al.³⁸ showed that a smaller particle size of filler contributes to the tensile strength, while the tensile modulus reduces. Interestingly, the compression and tensile moduli are nearly identical. Nonetheless, the tensile and elastic moduli of the specimens were of a similar magnitude to the compressive elastic modulus, meaning that resin D exhibited the highest elastic modulus valued at 20.76 GPa, and resin A had the lowest at 6.79 GPa.

3.1.3. Shear properties

The in-plane shear characteristics of the resin specimens were determined using a V-notched (Iosipescu) beam test. The testing principle can be idealized as a four-point flexural test with a rectangular specimen double-notched in the middle, as shown in Fig. 12a. Counteracting loads in the x and y directions (Fig. 12b) induce a bending moment, creating a high shear region in the middle of the specimen (Fig. 12c). The designed notches on the specimen affect the induced shear strain along the loading direction, generating uniform shear stress compared to conditions without the notches, which can lead to incline shear failure of the specimens (Fig. 12d)⁵¹. The shear stress can be determined by dividing the applied force by the cross-sectional area between the notches. The typical stress and corresponding crosshead displacement under shear loading are shown in Fig. 13. From the curves, it can be seen that the shear stiffness of the resins is almost equivalent in the initial stage, with resin B exhibiting the highest stiffness. Table 7 shows that, like the other mechanical tests, the inclusion of the oil-based catalyst provided better results in the shear testing. Among all resins, resin D recorded the highest shear strength, standing at 17.73 MPa,

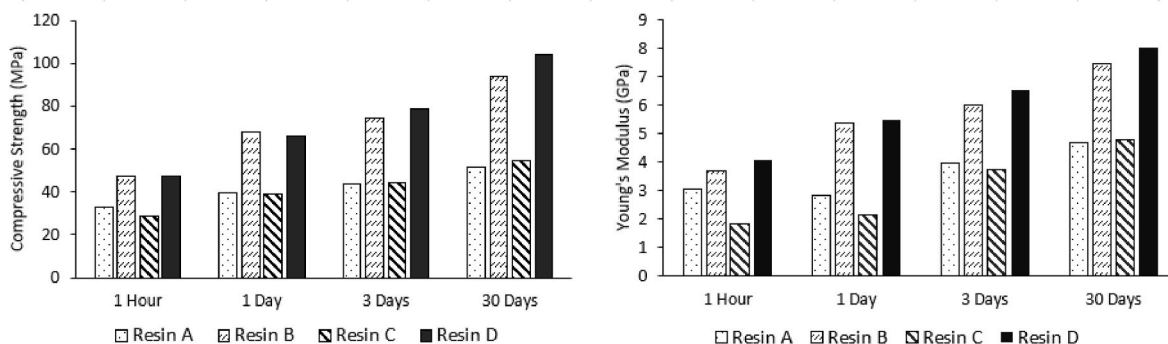


Fig. 8. Compressive strength and modulus of the resins over time.

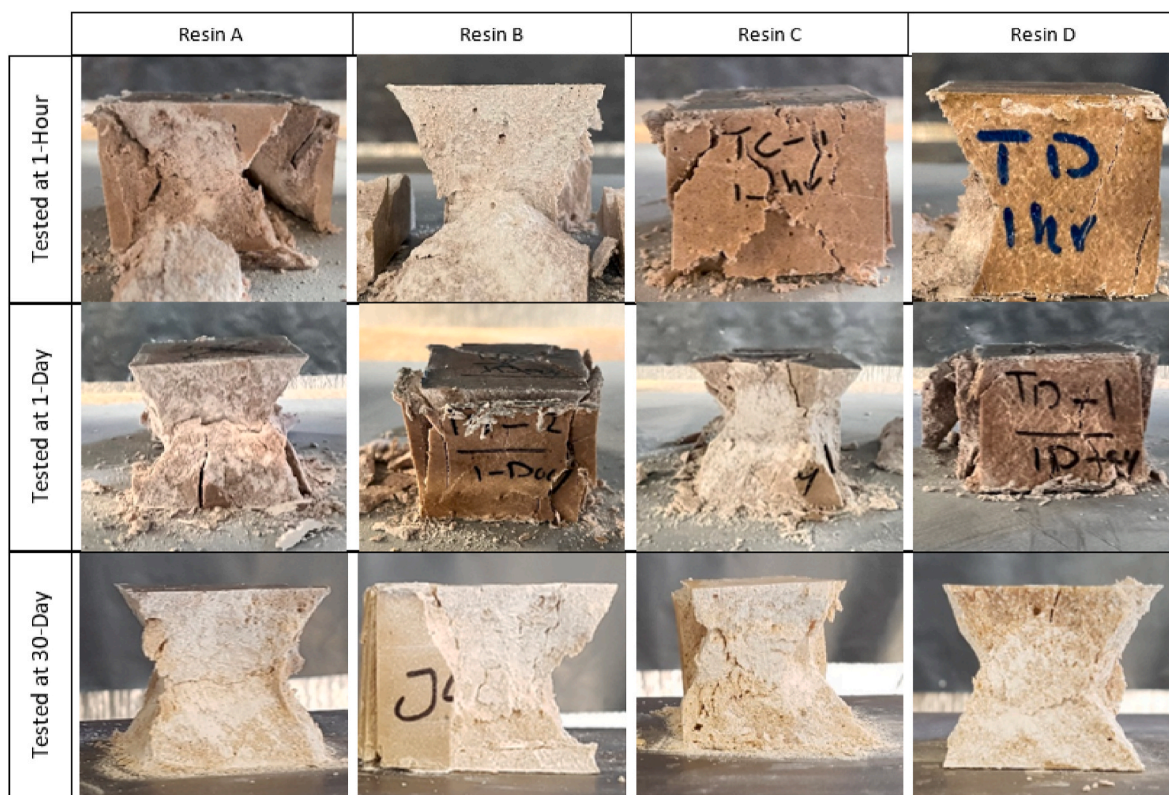


Fig. 9. Failure patterns of the resins under compression over curing periods.

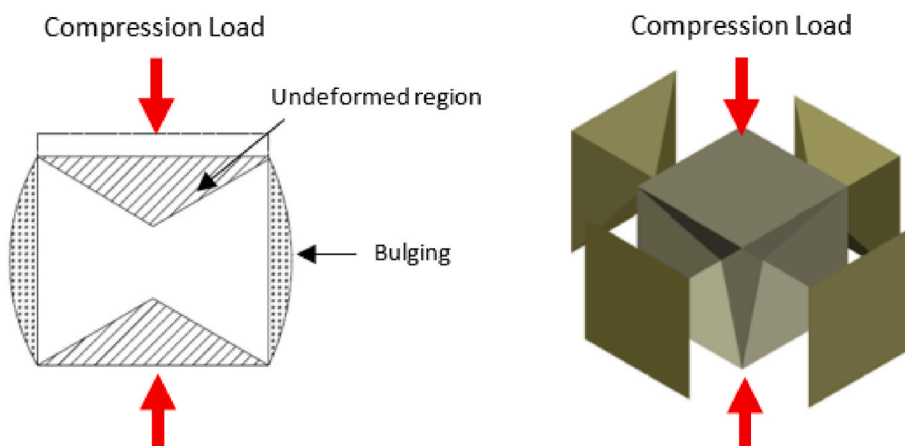


Fig. 10. Schematic of deformation and failure pattern under compression; adopted from Fiedler et al.⁴⁴

followed by resin B with a shear strength of 14.92 MPa. The shear strength of resins A and C were 9.15 MPa and 10.22 MPa, respectively. The compressive and shear strengths of resin D were 9.8% and 18.8% higher than that of resin B, respectively, while the tensile strength of resin D was 11.6% lower than that of resin B. This indicates that shear strength is also influenced by the filler particle size, and resins with coarser fillers exhibit higher shear strength.

3.2. Microstructure and thermal properties

The morphology and viscoelastic properties of resins A, B, C, and D were systematically investigated. Morphological analysis is critical as it provides a wide range of useful information during research and development and particularly during failure analysis. Many analytical techniques are available to study material morphology, including

microscopy, X-ray diffraction, thermal analysis, dynamic light scattering, porosimetry, and interferometry⁵². During morphological analysis, the size and shape of elements, voids, cracks, and the composition of morphological features are typically considered. The surface SEM images ($\times 24$ mag) are shown in Fig. 14. The SEM micrographs reveal the appearance of surface voids with diameters ranging up to 551 μm . Furthermore, the SEM images illustrate that resins A and C were more porous than resins B and D. Additionally, resin D exhibited a more consistent surface with less void density than resin B. Specifically, the maximum void diameter for B was 310 μm , while the maximum void diameter for D was 215 μm .

The study also included an analysis of the thermo-mechanical properties of the different chemical configurations, with all samples mixed and cured under the same conditions. Additionally, DSC experiments were conducted to examine the specimens cured at 30 min, 60

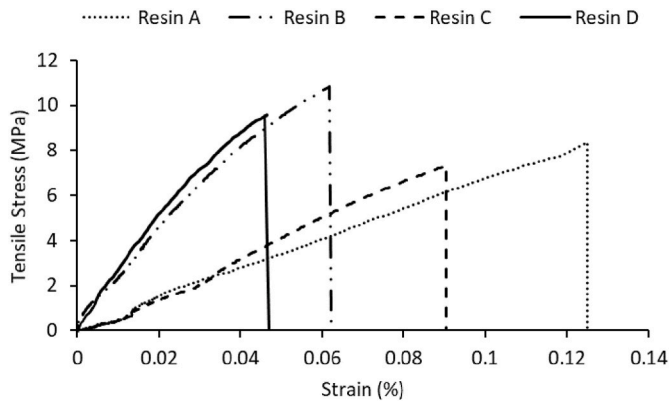


Fig. 11. Typical stress-strain behavior of the resins in tension.

Table 6
Summary of the tensile properties.

Parameters	Resin A	Resin B	Resin C	Resin D
Peak tensile stress (MPa)	8.35	10.81	7.29	9.55
Tensile modulus (GPa)	6.79	18.31	8.24	20.76
Strain at peak stress (%)	0.125	0.0618	0.0881	0.0466

min, 1 day, 7 days, and 30 days to determine the curing degrees. The typical results obtained from the DSC experiment for resin D are shown in Fig. 15. The figure indicates that the uncured resin D shows an exothermic peak after synthesis, while a quasi-linear response was observed after one day of synthesis. The reaction enthalpy can be calculated by integrating the area under the peak and the baseline⁵³. The curing percentage of the resins can be quantified using the heat flow-temperature curves obtained from DSC experiments and Eq. (1).

$$\% \text{ Cure} = \frac{[\Delta H_{\text{uncured}} - \Delta H_{\text{cured}}]}{\Delta H_{\text{uncured}}} \times 100\% \quad (1)$$

Where, $\Delta H_{\text{uncured}}$ is enthalpy under uncured resins and ΔH_{cured} is enthalpy under cured resins.

Table 7 presents the curing percentages of the resins at different time frames. The results show that after 30 min of synthesis, the maximum curing percentage was achieved for resin C at 91%, while resin B

exhibited the slowest early curing process at 54%. Furthermore, resins A and D cured 83% and 70% after 30 min of synthesis, respectively. Therefore, a comparison of the results shows that the curing degree of resins C and A in the early stage of synthesis was much higher than that of resins B and D. The high curing rates may lead to the generation of a significant volume of air bubbles being trapped in the specimen. After one day, all the samples were cured by over 80%, which can be considered as the critical time to ensure that the anchoring resin is sufficiently hardened. After 30 days, the resins reached their maximum curing degrees, which were 92%, 97%, 98%, and 99% for resin A, B, C,

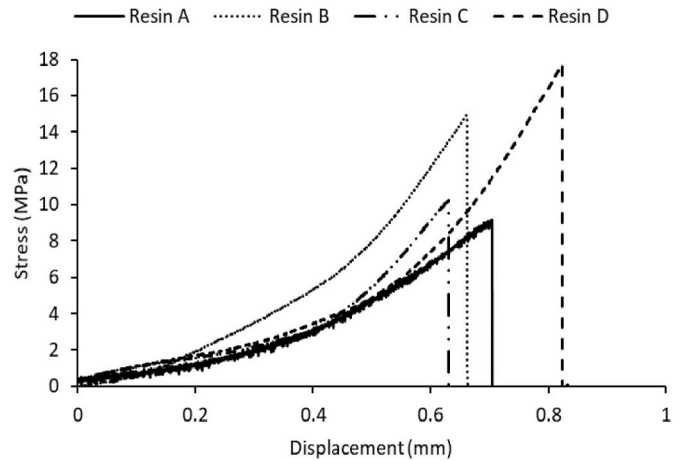


Fig. 13. Stress-displacement results of V-notched shear tests.

Table 7
Curing percentage of different resins over time.

Resins	Cured percentage [†] , %				
	30 Min.	1 Hour	1 Day	7 Day	30 Day
A	83	86	88	89	92
B	54	67	83	86	96
C	91	95	96	98	98
D	70	83	86	93	98

[†] Standard deviation $\pm 1.5\%$

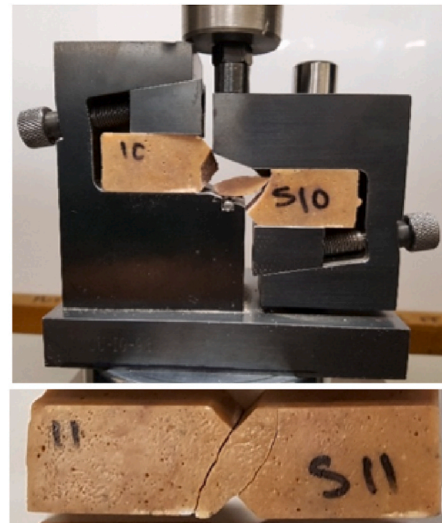
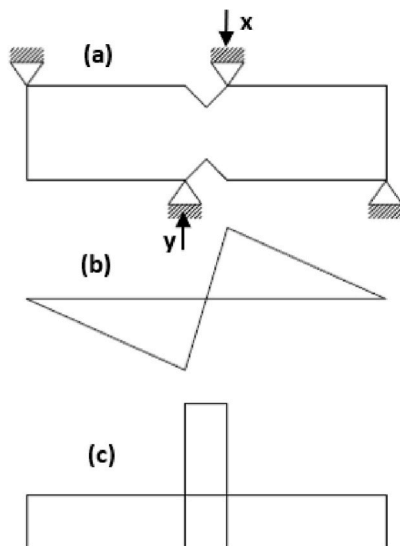


Fig. 12. (a) Schematic double notched specimen, (b) idealized bending moment diagram, (c) induced shear force and (d) typical failure after completion of the test; adopted from Merzkirch49.

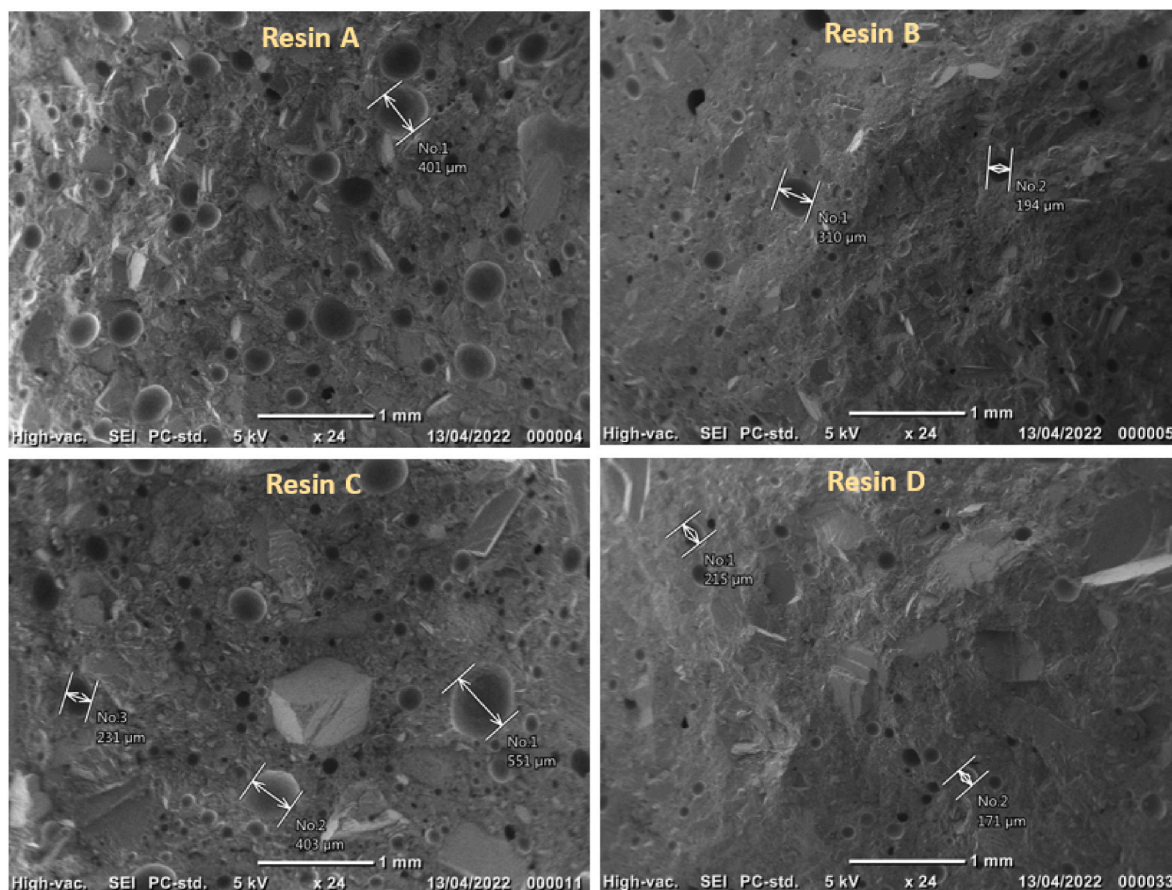


Fig. 14. SEM micrographs of resins A, B, C and D.

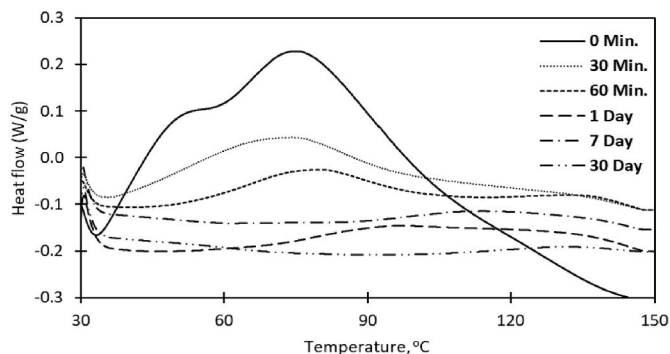


Fig. 15. DSC curing curves for resin D.

and D, respectively. There was no significant difference in the curing degrees of resins after 7 days, providing a solid platform for comparing the thermo-mechanical properties of the specimens.

Fig. 16 depicts the results obtained from the TGA experiments, and the respective decomposition temperatures are tabulated in Table 8. The experiments were carried out until 600 °C, and three main stages were identified. In stage (I), a significant mass loss was not observed at temperatures below 315 °C. In stage (II) (315 °C–420 °C), a rapid mass loss occurred due to the decomposition of the carbonate phase, which releases carbon dioxide⁵⁴. The decomposition temperatures of all resins were found to be similar at approximately 340 ± 7 °C. Hence, it can be inferred that the resins will not decompose unless exposed to high temperatures (>340 °C). In stage (III) (above 420 °C), all specimens showed a mass drop of about 30%, resulting in the evaporation of resin, as observed from the residue. Numerous studies have been conducted on

thermal gravimetric analysis (TGA) of unsaturated polyester resins all of which have yielded similar results where the rapid mass loss has been reported in range of 300–400 °C^{39,42,43,55,56}.

The storage modulus (E') obtained experimentally for resins A, B, C and D against temperature is shown in Fig. 17. According to the DMA tests summarized in Table 9, resin D exhibited the highest storage modulus of 7.64 ± 0.04 GPa, which is twice that of resin C at room temperature. Additionally, the storage moduli of resins A and B were 4.90 ± 0.01 and 6.22 ± 0.00 GPa, respectively at room temperature. From the storage modulus-temperature curves in Fig. 17, it is clear that the storage modulus of all the specimens decreases continuously with increasing temperature. The derivative of the storage modulus (E') with respect to temperature (T) provides valuable data. $(\frac{dE'}{dT}) = 0$ represents the corresponding temperature at which the specimens lose their mechanical properties rapidly. Table 9 shows that the critical temperature for resins A, B, C and D is in the range of 55–63 °C. At 80 °C, all the specimens lost over 70% of their storage modulus at room temperature. According to Fig. 17, the maximum storage modulus at 80 °C was observed in resin D. Comparison shows that resin D properties are more consistent than those of resins A, B and C, since it recorded a higher storage modulus from 0 °C to 120 °C.

3.3. Temperature related pull-out behaviors

The investigation of the bond capacity of chemically encapsulated rebars under elevated temperature using pull-out tests can generally be divided into two methods: (a) heating the specimen until a desired temperature is reached, and then increasing the load until the specimen debonds, and (b) subjecting the specimen to a specific load while continuously heating it until failure occurs. For this study, the first

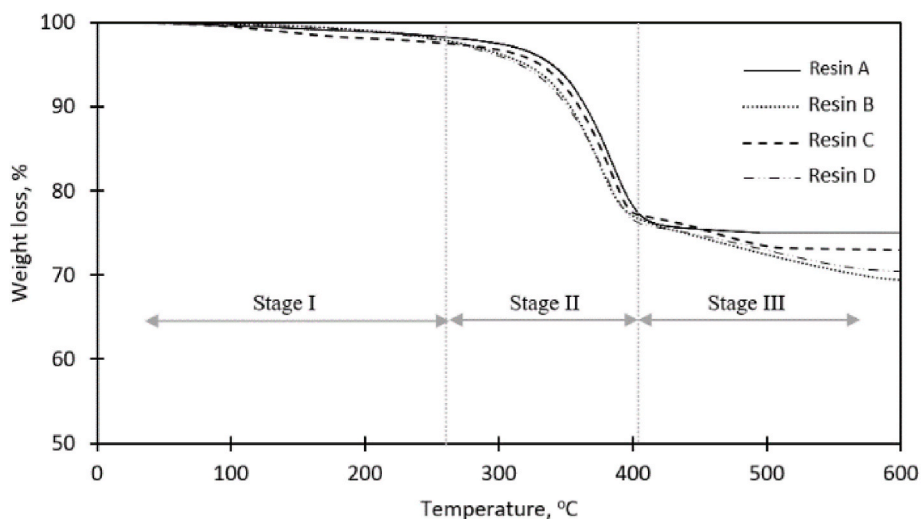


Fig. 16. TGA characterization curves of thermal decomposition for resins A, B, C and D.

Table 8
Thermal decomposition temperatures of all resins.

Resin type	Decomposition temperature (°C)
A	347.25 ^{±10.38}
B	336.81 ^{±12.47}
C	344.89 ^{±09.78}
D	331.44 ^{±6.15}

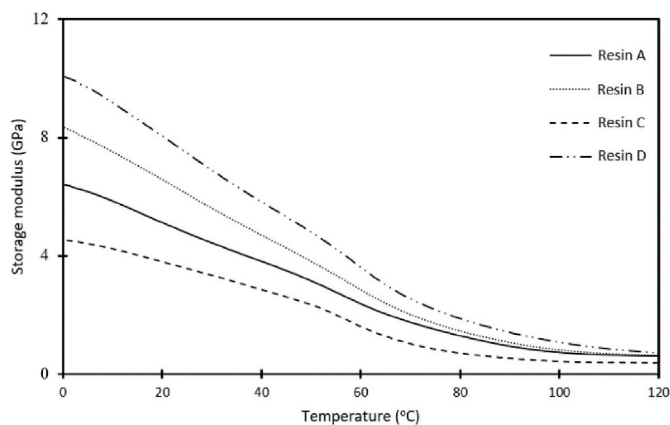


Fig. 17. DMA curves for the resins.

Table 9
Summary of the DMA test results.

Resin	Storage modulus at 23 °C (GPa)	Temperature (°C) at $\left(\frac{dE'}{dT}\right) = 0$
A	4.90 ^{±0.0154}	56.45 ^{±0.19}
B	6.22 ^{±0.00}	63.84 ^{±0.01}
C	3.64 ^{±0.02}	55.24 ^{±0.34}
D	7.64 ^{±0.04}	58.56 ^{±0.87}

technique was used. Fig. 18 displays the dimensions of the resin anchored-bolt specimens prepared for the pull-out tests, along with the positions of the thermocouples installed on the anchored bolts. Table 10 presents the temperature readings along the encapsulation length recorded during the heating and pull-out process. Temperature variation along the encapsulation depth for the specimen anchored using resin A is also illustrated in Fig. 19. A significant difference is observed between

the temperatures recorded in the heating chamber and those measured along the encapsulation length. This temperature variation is a function of two parameters: the first is the encapsulation depth, and the second is the chamber’s temperature. The recorded temperature decreases with increasing encapsulation length. Furthermore, at higher temperatures of the heating chamber, the temperature variation between the chamber and the thermocouples along the encapsulation length increases. For instance, the temperature variation between the chamber and T3 is 41.4 °C when the heater is set to 75 °C, while the variation increases to 170.3 °C when the chamber’s temperature is increased to 250 °C. The difference between the room temperatures shown in Table 10 is related to temperature changes during a day. Fig. 20 shows the bond resistance force versus displacement obtained from the pull-out tests. As shown, the bond strength of the encapsulated bolts decreases slightly when the temperature increases from room temperature to 75 °C; however, at higher temperatures (150 °C and 250 °C), the reduction is significant. For the bolt encapsulated by resin A, the peak bond strength decreases from 99.3 kN tested at room temperature (24 °C) to 92.8 kN for the specimen tested at 75 °C, representing a reduction of 6.5%. Increasing the temperature to 150 °C and 250 °C resulted in a reduction of 21.1% and 37.4% in the peak bond strength, respectively.

The pull-out tests of the specimens encapsulated using resin D at elevated temperatures showed similar behavior, but with a slightly higher rate of reduction compared to resin A. When the testing chamber temperature was increased to 75 °C, the peak bond strength reduced by 7.6% from 139.2 kN to 128.5 kN. A reduction of 31.3% and 42.5% was observed in the peak bond resistance strength when the chamber temperature was increased to 150 °C and 250 °C, respectively. The slightly higher rate of reduction in the bond strength of encapsulated specimens of resin D compared to that of resin A is supported by the results of DMA tests. The DMA result represented in Fig. 17 shows that the storage modulus of the resin D specimen is the highest at all temperatures. However, the rate of reduction in the storage modulus (which is the slope of the curve) is higher for resin D compared to resin A. From the DMA curves, it is evident that the storage modulus decreases from 9.9 GPa to 2.6 GPa as the temperature increases from 0 °C to 70 °C, resulting in a 7.3 GPa reduction with a 70 °C increase in temperature. On the other hand, the storage modulus of resin A reduces by 3.5 GPa in the same temperature range. Furthermore, the DMA plots indicate that the storage modulus of resins becomes relatively close (0.5–1 GPa) as the testing temperature approaches 100 °C. This investigation suggests that at higher temperatures, the filler type and their particle size do not significantly influence the mechanical properties of the anchoring resins compared to their influence at lower temperatures. At higher

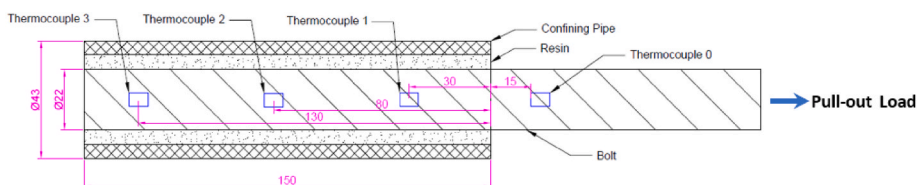


Fig. 18. Pull-out specimen with thermocouples.

Table 10
Temperature profiles along the encapsulation length.

Anchoring type	Recorded temperature by Thermocouples (°C)	Chamber Temperature			
		Room	75 °C	150 °C	250 °C
Resin A	T ₀	24.2 ± 0.6	54.4	102.1	164.7
	T ₁	0.6	39.1	69.6	110.2
	T ₂		35.6	61.7	91.1
	T ₃		33.6	56.2	79.7
Resin B	T ₁	22.8 ± 0.5	N/A	N/A	N/A
	T ₂				
	T ₃				
	T ₄				
Resin C	T ₁	22.4 ± 0.4	N/A	N/A	N/A
	T ₂				
	T ₃				
	T ₄				
Resin D	T ₀	20.4 ± 0.9	49.8	98.3	176.4
	T ₁		33.9	59.2	122.3
	T ₂		32	47.4	102.4
	T ₃		30.2	42.7	89.6
	T ₄				

temperatures, the matrix of the bonding materials rapidly loses its mechanical properties. The DMA tests conducted in the range of 55–63 °C for the resins used in this study determined the critical temperature.

Fig. 21 displays the ultimate bond capacity of specimens encapsulated with resins A, B, C, and D. At room temperature, the highest bonding capacity of 139.2 kN was observed for the bolt embedded using resin D. Resin B also exhibited a high level of bonding strength of 124.3 kN. For specimens prepared with resins A and C, debonding occurred once the pull-out load exceeded 99.3 kN and 106.4 kN, respectively. The results of mechanical tests correlate well with the pull-out test results, indicating a good correlation between compressive and shear strength and bonding properties. However, a weak correlation was found between the tensile characteristics of the resins and bonding. Kilic et al.¹² suggested that bond strength logarithmically increases with an increase in the compressive strength of grouts. In another study, Teymen and Kılıç¹⁴ concluded that grout mechanical characteristics affect shear and axial stress distributions along the embedment length. The bond strength of fully encapsulated rock bolts primarily depends on the shear characteristics of the bonding agent, including cohesion and internal friction angle, according to the failure modes of bolting systems. Fig. 22 illustrates the potential dependency of bond capacity and the mechanical properties of anchoring resins, which agrees with previous experimental and analytical research conducted to investigate rock bolting systems' failure modes. Shear-off/parallel shear failure is generally identified as the major mode of failure occurring at the bolt-grout

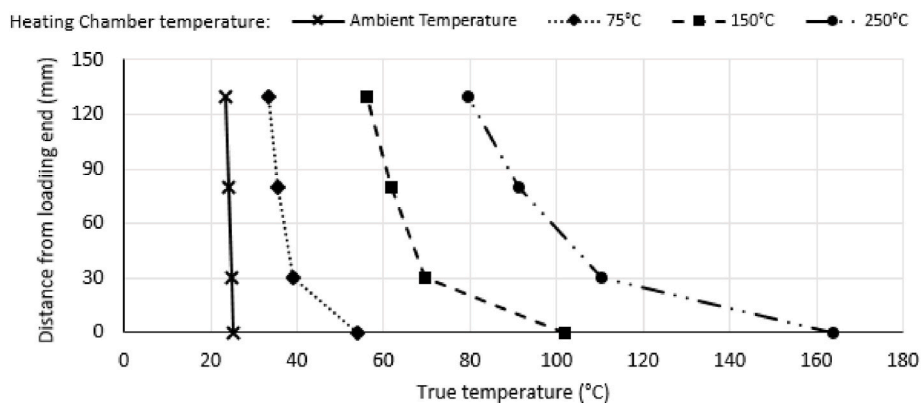


Fig. 19. Temperature variation along the encapsulation length for resin A.

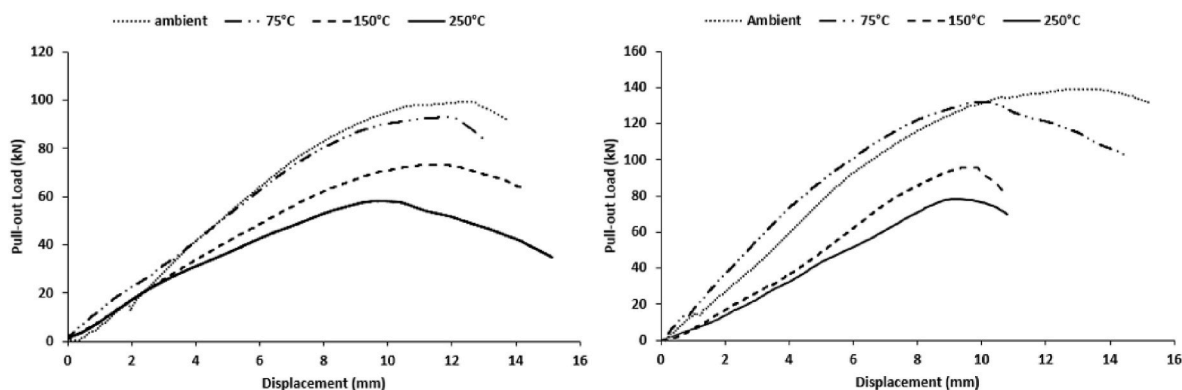


Fig. 20. Pull-out behavior of bolts encapsulated using resins A (left) and D (right) at elevated temperatures.

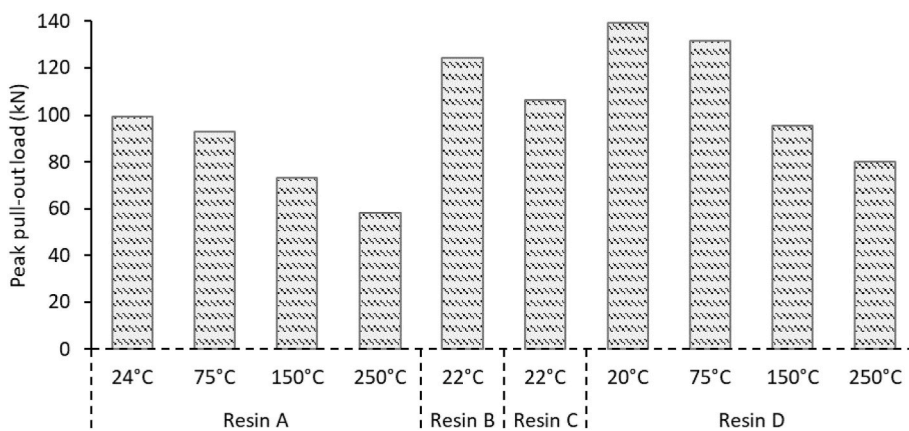


Fig. 21. Peak load measured for pull-out loads for bolts encapsulated resins A, B, C and D in different temperature conditions.

interface, given sufficient confinement pressure and surrounding media strength^{57,58}. Fig. 23 shows that the main failure mode of bolts was bond failure (slippage of bolts) occurring at the bolt-resin interface. However, a small degree of cone-shape failure was also observed. No radial cracks, signs of splitting failure, or bolt rupture were observed during testing programs.

The shrinkage and expansion properties of bonding agents can affect the interfacial bond strength of anchors. Benmokrane⁵⁹ demonstrated that the introduction of an expansion agent decreases the compressive strength of the grout but improves the shear bond resistance. It was noted that when cast in the compression test mold, the bonding agent is free to expand in one direction, while grout injection in the borehole provides higher normal stress resulting in higher bond strength. Further investigations revealed that although the compressive and shear strengths of resin C are 47% and 42% less than those of resin D, respectively (resins C and D comprise the same fillers type and size, and only the catalysts are different), the bonding strength of resin C is 23% less than that of resin D. Similarly, with the same filler content in resins A and B, the compressive and shear strengths of resin A are 44% and

38% less than those of resin B, respectively; however, the bonding strength of resin A is only 20% less than that of resin B. To the best of the authors' knowledge, this can be attributed to the observed expansion properties in resins A and C. Additionally, Fig. 24 clearly shows that resins A and C expanded during the curing of the molded compressive specimens, imposing higher normal forces on the bolt surface during pull-out testing, while resins B and D remained in the mold's shape.

3.4. Limitation of the study

This study provides a detailed experimental explanation of the pull-out performance of encapsulated rock bolts using unsaturated polyester resins under elevated temperature. However, some limitations need to be noted and studied further. The analysis of the results revealed that the temperature profile along the encapsulation length is non-uniform, and therefore, the bearing capacity should be distributed according to the temperature distribution. Moreover, the thermosetting characteristics of the anchoring resins cause the bonding deterioration process due to heating to be path-dependent, which needs to be taken into account.

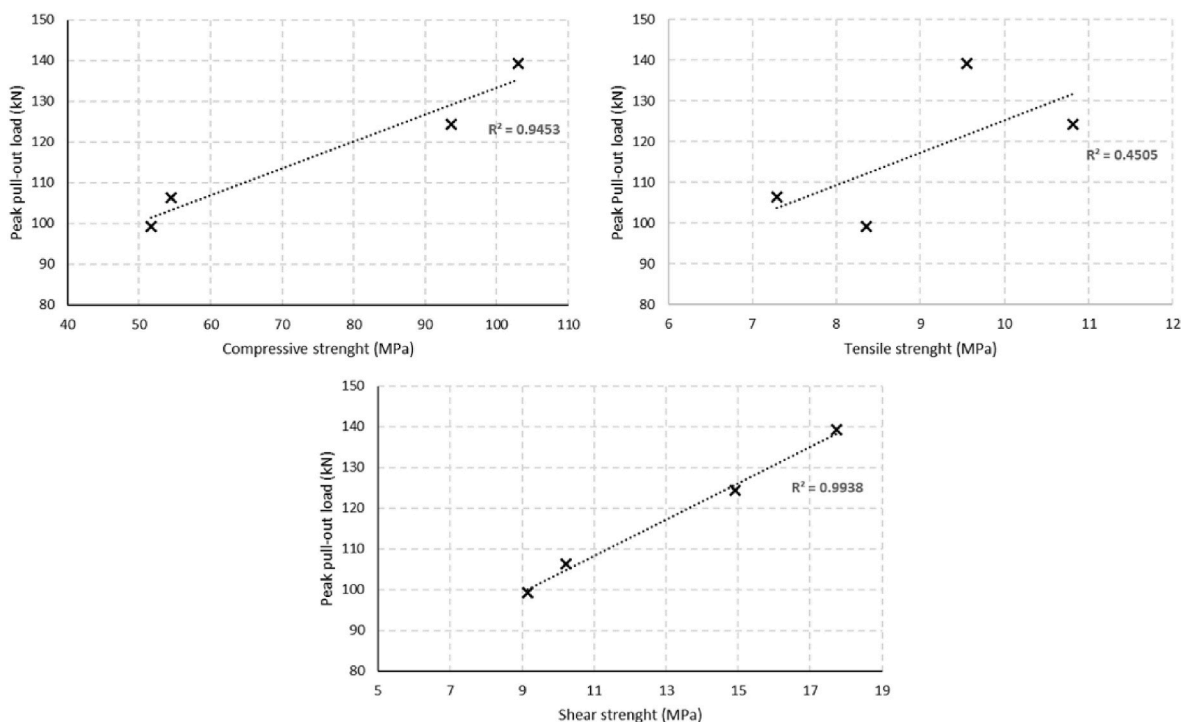


Fig. 22. Relationship between mechanical properties anchoring resins and the pull-out capacity of the encapsulated bolt.



Fig. 23. Failure of pull-out specimens embedded using resin A.

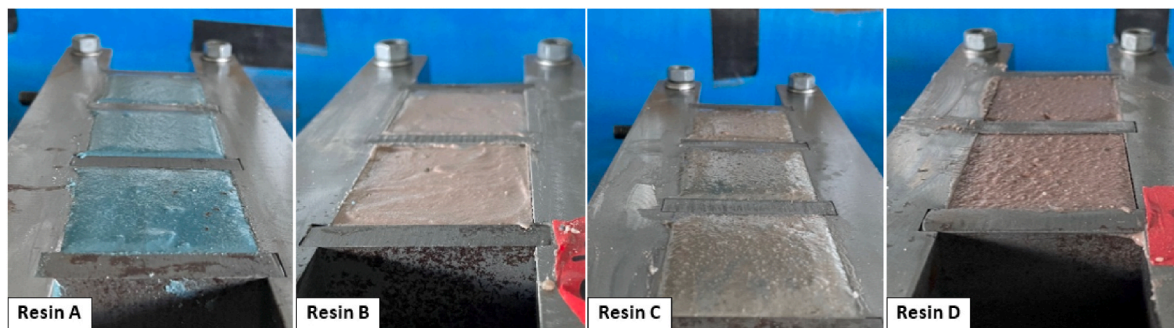


Fig. 24. Rising of the resins A and C before setting of the structure.

Further investigation is recommended to develop models and methods to address these limitations and improve the understanding of the performance of encapsulated rock bolts under elevated temperature conditions. In order to evaluate the long-term durability and reliability of the anchoring resins in actual working conditions, it is recommended to conduct further mechanical and pull-out tests specifically with higher encapsulation lengths installed in rock or concrete under elevated temperature and different heat exposure time. This will help gather data that can be used to improve the design and engineering of these materials.

4. Conclusions

Four two-component polyester-based anchoring resins were tested to characterize their mechanical, thermal, and bonding properties under various testing conditions. Two types of curing agents, including water-based and oil-based catalysts, were selected to mix with the resin matrices. The viscoelastic properties of the synthesized materials, as well as the compression, tensile, and shear properties, were comprehensively investigated. During the proof of concept, deformed rock bolts were encapsulated using the resins inside rifled steel pipes to determine the pull-out behavior of the bolting systems at room and elevated temperatures.

The TGA analysis revealed that the synthesized specimens decomposed at approximately 340 °C. DSC results showed that the curing degree of the specimens prepared by the water-based catalysts was slightly higher than that of oil-based specimens. Resins A and C reached 80% curing percentage in only 0.5 h, while resins B and D achieved this curing percentage in 1 h. According to the DMA results, the specimens' mechanical properties rapidly drop beyond 55–63 °C. Scanning electron microscopy micrographs illustrated that water-based catalyst used resins (A and C) are more porous compared to resins B and D. Thus, water-based agent was found to be the main reason causing the defects.

The compressive strength and elastic modulus of resins A, B, C, and D

were found to be within the range of 51–103 MPa and 4.71–8.03 GPa, respectively. Extensive voids were found in the specimens prepared using the water-based catalysts (A and C) compared to oil-based catalyst included resins (B and D), representing lower strength and modulus. The hybridization of filler particle size from micro to millimeter can lead to higher compressive strength and modulus.

The tested resins were able to achieve almost 50% of their ultimate compressive strength (tested at 30 days) after only 1 h. The main failure mode observed in the specimens under compression was cone-shaped rupture. While the bulging profile was observed in the compressive tests, the degree of bulging was found to be a function of the catalyst type and curing time. The tensile peak strength and modulus ranged from 7.29 to 10.81 MPa and 6.79–18.31 GPa, respectively. Unlike compressive properties, smaller filler particle size improved the tensile strength. However, the relationship between the tensile modulus and filler particle size was found to be similar to the compressive modulus. The shear strength of the resins ranged from 9.15 to 17.73 MPa. At ambient conditions, the bond strength of the anchored bolts ranged from 99.3 to 139.2 kN, and a good agreement was found between the compressive and shear properties of the anchoring resins and their corresponding bond resistance force.

To simulate a pull-out test at elevated temperature, a unique experimental set-up was developed. The results showed that a reduction of 6.6%–31.3% in the bond capacity of the bolts was measured when the chamber temperature reached 75 °C and 150 °C, respectively. Interestingly, the bolts encapsulated in resins A and D were able to acquire 62.6% and 57.5% bond strength at 250 °C compared to the initial strength.

Overall, the study provides a comprehensive and novel experimental framework to understand the behavior of chemically anchored rock bolts in the tunneling and underground mining industries. The effect of external fixtures of rock bolting systems, such as surface plates and nuts, on the temperature profile along the encapsulation length may also be of interest to other researchers, but was not considered in this study.

Therefore, it is recommended to undertake further studies on the performance of chemically anchored rock bolts after elevated temperature exposure over a significant time period.

Declaration of competing interest

The authors declare the following financial interests/personal relationships which may be considered as potential competing interests: Hadi Nourizadeh reports a relationship with University of Southern Queensland that includes: employment.

Data availability

Data will be made available on request.

Acknowledgment

The in-kind support from Jenmar Australia and Minova Australia is greatly acknowledged.

References

- Rastegarmanesh A, Mirzaghobanali A, McDougall K, et al. Axial performance of cementitious grouted cable bolts under rotation constraint scenarios. *Rock Mech Rock Eng.* 2022. <https://doi.org/10.1007/s00603-022-02950-4>. Published online.
- Contrafatto L, Cosenza R. Behaviour of post-installed adhesive anchors in natural stone. *Construct Build Mater.* 68:355-369. doi:10.1016/j.conbuildmat.2014.05.099.
- Xue-gui S, Xian-jie D, Hong-hu Y, Ben-kui L. Research of the thermal stability of structure of resin anchoring material based on 3D CT. *Int J Adhesion Adhes.* 2016;68:161-168. <https://doi.org/10.1016/j.ijadhadh.2016.03.005>.
- Pączkowski P, Puzska A, Gawdzik B. Investigation of degradation of composites based on unsaturated polyurethane resin and vinyl ester resin. *Materials.* 2022;15(4). <https://doi.org/10.3390/ma15041286>.
- Witt R, Cizek E. Effect of filler particle size on resins. *Ind Eng Chem.* 1954;46(8):1635-1639.
- Devi MS, Murugesan V, Rengaraj K, Anand P. Utilization of flyash as filler for unsaturated. *J Appl Polym Sci Polym Sci.* 1998;69(7):1385-1391. [https://doi.org/10.1002/\(SICI\)1097-4628\(19980815\)69:7<1385::AID-APP13>3.0.CO;2-T](https://doi.org/10.1002/(SICI)1097-4628(19980815)69:7<1385::AID-APP13>3.0.CO;2-T).
- Rahman GMS, Aftab H, Islam MS, Zobayer M, Mukhlis B, Ali F. Enhanced physico-mechanical properties of polyester resin film using CaCO₃ filler. *Fibers Polym.* 2016;17(1):59-65. <https://doi.org/10.1007/s12221-016-5612-y>.
- Bagherzadeh A, Jamshidi M, Monemian F. Investigating mechanical and bonding properties of micro/nano filler containing epoxy adhesives for anchoring steel bar in concrete. *Construct Build Mater.* 240. doi:10.1016/j.conbuildmat.2019.117979.
- Fu M, Liu S, Jia H, He D. Experimental study of an orientation and resin-lifting device for improving the performance of resin-anchored rock bolts. *Rock Mech Rock Eng.* 2019;53(1):211-231. <https://doi.org/10.1007/s00603-019-01906-5>.
- Rastegarmanesh A, Mirzaghobanali A, McDougall K, et al. Axial response of resin encapsulated cable bolts in monotonic and cyclic loading. *Can Geotech J.* 2023. <https://doi.org/10.1139/cgj-2022-0379>. Published online.
- Nourizadeh H, Williams S, Mirzaghobanali A, McDougall K, Aziz N, Serati M. Axial behaviour of rock bolts-part (A) Experimental study. In: *Recource Operator.* 2021.
- Kılıc A, Yasar E, Celik AG. Effect of grout properties on the pull-out load capacity of fully grouted rock bolt. *Tunn Undergr Space Technol.* 2002;17:355-362.
- Cao C, Nemcik J, Aziz N, Ren T. Analytical study of steel bolt profile and its influence on bolt load transfer. *Int J Rock Mech Min Sci.* 2013;60:188-195. <https://doi.org/10.1016/j.ijrmms.2012.12.013>.
- Teymen A, Kılıc A. Effect of grout strength on the stress distribution (tensile) of fully-grouted rockbolts. *Tunn Undergr Space Technol.* 2018;77:280-287. <https://doi.org/10.1016/j.tust.2018.04.022>.
- Ho D, Bost M, Rajot J. Numerical study of the bolt-grout interface for fully grouted rockbolt under different confining conditions. *Int J Rock Mech Min Sci.* 2019;119 (September 2017):168-179. <https://doi.org/10.1016/j.ijrmms.2019.04.017>.
- chun Ma H, hui Tan X, zhong Qian J, liang Hou X. Theoretical analysis of anchorage mechanism for rock bolt including local stripping bolt. *Int J Rock Mech Min Sci.* 2019;122(December 2018), 104080. <https://doi.org/10.1016/j.ijrmms.2019.104080>.
- Liu S, He D, Fu M. Experimental investigation of surrounding-rock anchoring synergistic component for bolt support in tunnels. *Tunn Undergr Space Technol.* 2020;104. <https://doi.org/10.1016/j.tust.2020.103531>.
- Wang W, Pan Y, Xiao Y. Synergistic resin anchoring technology of rebar bolts in coal mine roadways. *Int J Rock Mech Min Sci.* 2022;151. <https://doi.org/10.1016/j.ijrmms.2022.105034>.
- Liu X, Yao Z, Xue W, Wang X, Huang X, Li Y. Experimental study of the failure mechanism of the anchorage interface under different surrounding rock strengths and ambient temperatures. *Adv Civ Eng.* 2021;2021:1-17. <https://doi.org/10.1155/2021/6622418>.
- Dudek D, Kadela M. Pull-out strength of resin anchors in non-cracked and cracked concrete and masonry substrates. *Procedia Eng.* 161:864-867. doi:10.1016/j.proeng.2016.08.734.
- Hyett AJ, Bawden WF, Reichert RD. The effect of rock mass confinement on the bond strength of fully grouted cable bolts. *Int Rock Mech Min Sci Geomech Abstr.* 1992;29 (5):503-524.
- Benmokrane B, Chennouf A, Mitri HS. Laboratory evaluation of cement-based grouts and grouted rock anchors. *Int J Rock Mech Min Sci Geomech Abstr.* 1995;32(7):633-642.
- Yokota Y, Zhao Z, Nie W, Date K, Iwano K, Okada Y. Experimental and numerical study on the interface behaviour between the rock bolt and bond material. *Rock Mech Rock Eng.* 2019;52:869-879. <https://doi.org/10.1007/s00603-018-1629-4>.
- Wang M, Hu Y, Jiang C, Wang Y, Liu D, Tong J. Mechanical characteristics of cement-based grouting material in high-geothermal tunnel. *Materials.* 2020;13(7). <https://doi.org/10.3390/ma13071572>.
- Jahani Y, Baena M, Barris C, Perera R, Torres L. Influence of curing, post-curing and testing temperatures on mechanical properties of a structural adhesive. *Construct Build Mater.* 2022;324. <https://doi.org/10.1016/j.conbuildmat.2022.126698>.
- Michel M, Ferrier E. Effect of curing temperature conditions on glass transition temperature values of epoxy polymer used for wet lay-up applications. *Construct Build Mater.* 231. doi:10.1016/j.conbuildmat.2019.117206.
- Wang S, Stratford T, Reynolds TPS. Linear creep of bonded FRP-strengthened metallic structures at warm service temperatures. *Construct Build Mater.* 283. doi:10.1016/j.conbuildmat.2021.122699.
- Yu C, Tian W, Zhang C, Chai S, Cheng X, Wang X. Temperature-dependent mechanical properties and crack propagation modes of 3D printed sandstones. *Int J Rock Mech Min Sci.* 146. doi:10.1016/j.ijrmms.2021.104868.
- Laredo M, Theoretical R, Fluminense UF, Passo R. *Effect of Temperature on the Mechanical Properties of Polymer Mortars.* 2012;15(4):645-649. <https://doi.org/10.1590/S1516-14392012005000091>.
- Pinoteau N, Heck J V, Rivillon P, et al. Prediction of failure of a cantilever-wall connection using post-installed rebars under thermal loading. *Eng Struct.* 56:1607-1619. doi:10.1016/j.engstruct.2013.07.028.
- Amine M, François Caron J, Pinoteau N, Forêt G. International Journal of Adhesion and Adhesives Mechanical behavior of adhesive anchors under high temperature exposure : experimental investigation. *Int J Adhesion Adhes.* 2017;78(July):200-211. <https://doi.org/10.1016/j.ijadhadh.2017.07.004>.
- Al-Mansouri O, Mege R, Pinoteau N, Guillet T, Rémond S. Influence of testing conditions on thermal distribution and resulting load-bearing capacity of bonded anchors under fire. *Eng Struct.* 192:190-204. doi:10.1016/j.engstruct.2019.04.099.
- European Assessment Document E. *Systems for Post-Installed Rebars Connections with Mortar*; 2020. <http://www.eota.eu>.
- Lakhani H, Hofmann J. A numerical method to evaluate the pull-out strength of bonded anchors under fire. In: *3rd Int Symp Connect between Steel Concr.* 2017. Published online.
- Yang H, Lee LJ. Comparison of unsaturated polyester and vinyl ester resins in low temperature polymerization. *J Appl Polym Sci.* 2001;79(7):1230-1242. [https://doi.org/10.1002/1097-4628\(20010214\)79:7<1230::AID-APP100>3.0.CO;2-2](https://doi.org/10.1002/1097-4628(20010214)79:7<1230::AID-APP100>3.0.CO;2-2).
- McAlvin JE, Dowd ZS, Kinnin LF, et al. *Next Generation Novolac Epoxy Vinyl Ester Resins for Heat Resistant Composites.* CAMX. Compos Adv Mater Expo; 2016. Published online 2016.
- yun Fu S, qiao Feng X, Lauke B, wing Mai Y. Effects of particle size , particle/matrix interface adhesion and particle loading on mechanical properties of particulate – polymer composites. *Compos Part B.* 2008;39:933-961. <https://doi.org/10.1016/j.compositesb.2008.01.002>.
- Mourad AHI, Abu-Jdayil B, Hassan M. Mechanical behavior of Emirati red shale fillers/unsaturated polyester composite. *SN Appl Sci.* 2020;2(3):1-9. <https://doi.org/10.1007/s42452-020-2284-4>.
- Lin Y, Jiang S, Gui Z, Li G, Shi X. Synthesis of a novel highly effective flame retardant containing multivalent phosphorus and its application in unsaturated polyester resins. *RSC Adv.* 2016;6:86632-86639. <https://doi.org/10.1039/C6RA19798A>.
- Alif Z, Halim A, Azizi M, et al. Effect of silica aerogel – aluminium trihydroxide hybrid filler on the physio-mechanical and thermal decomposition behaviour of unsaturated polyester resin composite. *Polym Degrad Stabil.* 2020;182, 109377. <https://doi.org/10.1016/j.polydegradstab.2020.109377>.
- Preghenella M, Pegoretti A, Migliareti C. Thermo-mechanical characterization of fumed silica-epoxy nanocomposites. *Polymer (Guildf).* 46(26):12065-12072. doi:10.1016/j.polymer.2005.10.098.
- Tabatabai H, Janbaz M, Nabizadeh A. Mechanical and thermo-gravimetric properties of unsaturated polyester resin blended with FGD gypsum. *Construct Build Mater.* 2018;163:438-445. <https://doi.org/10.1016/j.conbuildmat.2017.12.041>.
- Lavoratti A, Cristine L, José A. Dynamic-mechanical and thermomechanical properties of cellulose nanofiber/polyester resin composites. *Carbohydr Polym.* 2016;136:955-963. <https://doi.org/10.1016/j.carbpol.2015.10.008>.
- Fiedlera B, Hojia M, Ochiaia S, Schulte K, Andoc M. Failure behavior of an epoxy matrix under different kinds of static loading. *Compos Sci Technol.* 2001;61.
- Yeon JH, Lee HJ, Yeon J. Deformability in unsaturated polyester resin-based concrete: effects of the concentration of shrinkage-reducing agent and type of filler. *Materials.* 2020;13(3). <https://doi.org/10.3390/ma13030727>.
- Gary G, Bailly P. Behaviour of quasi-brittle material at high strain rate. Experiment and modelling. *Eur J Mech Solid.* 1998;17(3).
- Cai M, Hou PY, Zhang XW, Feng XT. International journal of rock mechanics and mining sciences post-peak stress. *Strain curves of brittle hard rocks under axial-strain-controlled loading.* 2021;147(September).
- Gong F, Zhang P, Xu L. Damage constitutive model of brittle rock under uniaxial compression based on linear energy dissipation law. *Int J Rock Mech Min Sci.* 2022;160(September 2021), 105273. <https://doi.org/10.1016/j.ijrmms.2022.105273>.
- Chen W, Lu F, Cheng M. Tension and compression tests of two polymers under quasi-static and dynamic loading. *Polym Test.* 2002;21.

- 50 Sampath C, Lokuge W, Islam M. Compressive strength characterization of polyester based fillers. *Adv Mater Res*. 2012;410:32–35. <https://doi.org/10.4028/www.scientific.net/AMR.410.32>.
- 51 Merzkirch M. *Mechanical Characterization Using Digital Image Correlation*. Cham: Springer; 2022. https://doi.org/10.1007/978-3-030-84040-2_3.
- 52 Popelka A, Zavahir S, Habib S. Morphology analysis. In: *Polymer Science and Innovative Applications: Materials, Techniques, and Future Developments*. 2020:21–68.
- 53 Flynn JH. Analysis of DSC results by integration. *Thermochim Acta*. 1993;217: 129–149.
- 54 Cultrone G, Rodriguez-Navarro C, Sebastian E, Cazalla O, Dela Torre MJ. Carbonate and silicate phase reactions during ceramic firing. *Eur J Mineral*. 2001;13(3): 621–634.
- 55 Lin Y, Yu B, Jin X, Hu Y. Study on thermal degradation and combustion behavior of flame retardant unsaturated polyester resin modified with a reactive phosphorus containing monomer. *RSC Adv*. 2016;6:49633–49642. <https://doi.org/10.1039/C6RA06544A>.
- 56 Lin Y, Jiang S, Hu Y, Chen G, Shi X, Peng X. Hybrids of aluminum hypophosphite and ammonium polyphosphate : highly effective flame retardant system for unsaturated polyester resin. *Polymer (Guildf)*. 2018;39(5):1763–1770. <https://doi.org/10.1002/polb.24128>.
- 57 Cao C, Ren T, Cook C, Cao Y. Analytical approach in optimising selection of rebar bolts in preventing rock bolting failure. *Int J Rock Mech Min Sci*. 2014;72:16–25. <https://doi.org/10.1016/j.ijrmms.2014.04.026>.
- 58 Cui G, Zhang C, Pan Y, Deng L, Zhou H. Laboratory investigation into effect of bolt profiles on shear behaviors of bolt-grout interface under constant normal stiffness (CNS) conditions. *J Rock Mech Geotech Eng*. 2020;12(6):1234–1248. <https://doi.org/10.1016/j.jrmge.2020.03.010>.
- 59 Benmokrane B, Zhang B, Chenouf A. Tensile properties and pullout behaviour of AFRP and CFRP rods for grouted anchor applications. *Construct Build Mater*. 2000;14: 157–170.